Hydrol. Earth Syst. Sci. Discuss., 11, 1253–1300, 2014
www.hydrol-earth-syst-sci-discuss.net/11/1253/2014/
doi:10.5194/hessd-11-1253-2014

Hydrology and Earth System Sciences
Open Access
Discussions

Diagnostic calibration of a hydrological model in an alpine area

Z. He[1], F. Tian[1], H. C. Hu[1], H. V. Gupta[2], and H. P. Hu[1]

[1]State Key Laboratory of Hydroscience and Engineering, Department of Hydraulic Engineering, Tsinghua University, Beijing, 100084, China
[2]Department of Hydrology and Water Resources, The University of Arizona, Tucson, Arizona, 85721, USA

Received: 19 November 2013 – Accepted: 10 January 2014 – Published: 23 January 2014

Correspondence to: F. Tian (tianfq@tsinghua.edu.cn)

Published by Copernicus Publications on behalf of the European Geosciences Union.

Abstract

Hydrological modeling depends on single- or multiple-objective strategies for parameter calibration using long time sequences of observed streamflow. Here, we demonstrate a diagnostic approach to the calibration of a hydrological model of an alpine area in which we partition the hydrograph based on the dominant runoff generation mechanism (groundwater baseflow, glacier melt, snowmelt, and direct runoff). The partitioning reflects the spatiotemporal variability in snowpack, glaciers, and temperature. Model parameters are grouped by runoff generation mechanism, and each group is calibrated separately via a stepwise approach. This strategy helps to reduce the problem of equifinality and, hence, model uncertainty. We demonstrate the method for the Tailan River basin (1324 km^2) in the Tianshan Mountains of China with the help of a semi-distributed hydrological model (THREW).

1 Introduction

1.1 Background

Parameter calibration has been singled out as one of the major issues in the application of hydrological models (Johnston and Pilgrim, 1976; Gupta and Sorooshian, 1983; Beven and Binley, 1992; Boyle et al., 2000). Commonly, one or more objective functions are selected as criteria to evaluate the similarity between observed and simulated hydrographs (Nash and Sutcliffe, 1970; Brazil, 1989; Gupta et al., 1998; van Griensven and Bauwens, 2003). As model complexity increases, parameter dimensionality also increases significantly. For this reason, automatic calibration procedures have been developed to identify the optimal parameter set (Gupta and Sorooshian, 1985; Gan and Biftu, 1996; Vrugt et al., 2003a, b). However, given the limited capability of process understanding and measurement technologies, models have been developed that include different parameter sets within a chosen space that may acceptably reproduce

the observed aspects of the catchment system (Sorooshian and Gupta, 1983; Beven and Freer, 2001). This phenomenon has been called "equifinality", and it causes uncertainty in simulation and prediction (Duan et al., 1992; Beven, 1993, 1996). The "equifinality" issue in hydrology calls for methods that are powerful enough to evaluate and correct models and therefore must be "diagnostic", i.e. capable of pointing to what degree a realistic representation of the real world has been achieved and how the model should be improved (Spear and Hornberger, 1980; Gupta et al., 1998, 2008).

However, traditional regression-based model evaluation strategies (e.g. based on the use of Mean Squared Error or Nash Sutcliffe Efficiency as performance criteria) are demonstrably poor in their ability to identify the roles of various model components or parameters in the model output (Van Straten and Keesman, 1991), which is due in part to the loss of meaningful information when projecting from the high dimension of the data set down to the low (often one) dimension of the measure (Yilmaz et al., 2008; Gupta et al., 2009). A diagnostic evaluation method should match the number of unknowns (parameters) with the number of pieces of information by making use of multiple measures of model performance (Gupta et al., 1998, 2008, 2009; Yilmaz et al., 2008). One way to exploit hydrological information is to analyze the spatiotemporal characteristics of hydrological variables that can be related to specific hydrological processes in the form of "signature indices" (Richter et al., 1996; Sivapalan et al., 2003; Yilmaz et al., 2008). Ideally, a "signature" should represent some "invariant" property of the system, be readily identifiable from available data, directly reflect some system function, and be maximally related to some "structure" or "parameter" in the model.

Attention to hydrological signatures, therefore, constitutes the natural basis for model diagnosis (Gupta et al., 2008). Placed in this context, the body of literature on the topic is indeed large. Yadav et al. (2007) used similarity indices and hydrological signatures (runoff ratio and slope of the flow duration curve – FDC) to classify catchments. Shamir et al. (2005a) described a parameter estimation method based on hydrograph descriptors (total flow, range between the extreme values, monthly rising limb density of the hydrograph, monthly maximum flow and negative/positive change) that characterize

dominant streamflow patterns at three time scales (monthly, yearly, and record extent). Detenbeck et al. (2005) calculated several hydrologic indices including daily flow indices (mean, median, coefficient of variation and skewness), overall flood indices (flood frequency, magnitude, duration, and flood timing of various levels), low flow variables (mean annual daily minimum), and ranges of flow percentiles to study the relationship of the streamflow regime to watershed characteristics. Shamir et al. (2005b) presented two streamflow indices to describe the shape of the hydrograph (rising/declining limb density, i.e. RLD and DLD) for parameter estimation in 19 basins. Farmer et al. (2003) evaluated the climate, soil and vegetation controls on the variability of water balance through the following four signatures: gradient of the annual yield frequency graph, average yield over many years for each month, FDC and magnitude and shape of the hydrograph. Jothityangkoon et al. (2001) proposed a downward approach to evaluate the model's performance against appropriate signatures at progressively refined time scale. Signatures that governed the evaluation of model complexity were the interannual variability, mean monthly variation in runoff (called regime curve), and the FDC.

Generally, the reported signatures have the following two characteristics: (1) they concentrate on the extraction of the hydrologically meaningful information contained in the hydrograph, and (2) they focus on either the entire study period or a special continuous section of the entire period. However, they have occasionally considered the temporal variability of the runoff components and the dominance of different runoff generation mechanisms during different periods (Boyle et al., 2000). Arguably, the signatures in common use today insufficiently exploit the hydrograph information in the time dimension or in relation to the dominant runoff generation mechanisms.

For the alpine areas, on one hand, the hydrological processes are usually more complex with snow/glacier melting and possibly soil freezing/thawing than those in warmer areas, which implies a larger dimension of parameter (R^{P}) in the corresponding hydrological models. On the other hand, measured data set useful for model identification is usually limited due to the sparse gauged network, which produces a small measurement dimension (R^{M}) far lower than R^{P}. This intensifies the issue of equifinality in

parameter identification. To address this problem, related studies are putting efforts into two directions: the first one is to reduce the calibrated R^P by estimating part parameters based on basin characteristics a priori. For example, Gurtz et al. (1999) proposed a parameterization method based on elevation, slop and shading derived from basin terrain. Gomez-Landesa and Rango (2002) obtained model parameters of ungauged basins from gauged basins by basin size, proximity of location and shape similarities; Eder et al. (2005) estimated most of the parameters a priori from basin physiography before an automatic calibration is applied. The parameterization method may involve some uncertainties but be useful for the determination of insensitive parameters. The second direction is expanding the R^M by exploiting information from available data. For instance, Dunn and Colohan (1999) used baseflow data as an additional criteria for model evaluation. Mendoza et al. (2003) exploited recession-flow data to estimate hydraulic parameters. Stahl et al. (2008) used glacier mass balance information combined with stream hydrographs to constrain the melt factors, and used the volume-area scaling approach to estimate changes in glacier area. The results indicate that glacier mass balance can reduce uncertainty both in parameter calibration and predictions. Konz and Seibert (2010) combined glacier mass balance data with discharge to find the appropriate parameter sets generated by Monte Carlo analyses. Schaefli and Huss (2011) integrated seasonal point glacier mass balance information for model calibration by modifying the GSM-SOCONT model. They used the winter accumulation and annual balance to determine the snow accumulation correction factor, snow melt factor and temperature lapse rate. Enough seasonal glacier information is a pre-requisite for this method. Jost et al. (2012) introduced glacier volume loss calculated by digital elevation models to calibrate hydrologic model. Uncertainty analyses by a generalized likelihood uncertainty estimation (GLUE) procedure demonstrated that glacier volume is helpful to reduce parameter uncertainty even in catchments where lack mass balance data. Knowledge acquired from these researches is that using additional information (baseflow and glacier mass) can reduce parameter uncertainty effectively, which expand the R^M significantly.

Hydrograph separation could be another way to expand R^M. Studies have confirmed that a hydrograph can be dominated by various components in different response periods (Haberlandt et al., 2001; Eder et al., 2005). Information about the dominant hydrological processes contained in a hydrograph can be extracted by hydrograph separation or partitioning; this has long been a topic of interest in the science of hydrology. Several methods have been proposed (Pinder and Jones, 1969; McCuen, 1989; Nathan, 1990; Vivoni et al., 2007). In general, these can be divided into graphical methods, analytical methods, empirical methods, geochemical methods and automated program techniques (Nejadhashemi et al., 2009). Most of them primarily focus on the partitioning of baseflow and are not capable of identifying more than two components. With the advance of isotope methods, multi-component hydrograph separation models have been developed. However, these models should be run on an extended period of time (usually a minimum of one hydrologic year) in order for the assumption that the isotopes of components are conserved to hold (Hooper and Shoemaker, 1986) and call for volumes of field data that are difficult to acquire in poorly gauged alpine basins.

1.2 Objectives and scope

In this paper, we explore the benefits of partitioning the hydrograph into several parts, each related to a different runoff generation mechanism. The parameter groups controlling each mechanism can then be calibrated for the corresponding hydrograph partition, and the deficiencies of the model can be diagnosed by evaluating the model simulations associated with each partition. We demonstrate the potential of this approach in an alpine area where streamflow is the result of complex runoff generation processes arising from combinations of storm events and snow/glacier melt. The influence of each of the runoff components (groundwater baseflow, glacier melt, snowmelt, and direct storm-runoff) varies in time and can be determined by an analysis of the dynamic spatiotemporal information in the available data series.

The paper is organized as follows. Section 2 contains a description of the geographic and hydrological characteristics of the study basin, including the main data sources and some data preprocessing methods. Section 3 details the proposed method of hydrograph partitioning and parameter calibration based on a semi-distributed model coupled with the temperature-index method. Section 4 presents the main simulation result and discusses the possible sources of uncertainty in these results. Section 5 provides a summary of this study and discusses further applications of the partitioning strategy.

2 Study area and data

2.1 Overview of the study area

The studied alpine watershed (Tailan River basin, TRB) is located in the Xinjiang Uygur Autonomous Region of northwestern China and extends from 41°35′ N to 42°05′ N and 80°04′ E to 80°35′ E, covering a drainage area of 1324 km^2. Basin elevation ranges from 1600 m to 7100 m a.s.l. The Tailan River flows across the basin from north to south (Fig. 1). In high-altitude regions, the land is covered by snow and glaciers throughout the year. Glacier coverage occupies approximately 33 % of the total basin area (Fig. 1). The glacier coverage stretches from approximately 3000 m to 7100 m a.s.l. and mainly exists at an altitude range of 4000 m to 5000 m a.s.l. Glacier melt and snowmelt form runoffs as long as the temperature is at a certain threshold and provide the primary source for downstream discharge.

TRB is a heavily studied alpine watershed in northwestern China. The relevant literature (Kang and Zhu, 1980; Shen et al., 2003; Xie et al., 2004; Gao et al., 2011; Sun et al., 2012) are reviewed, and the main conclusions about its hydrometeorological characteristics are summarized as follows:

1. The climate condition presents strong altitudinal variability. The mean annual precipitation in higher mountain areas is approximately 1200 mm (Kang et al., 1980), while it is approximately 180 mm in the outlet plain area (Xie et al., 2004). The mean annual temperature ranges from below 0 °C in mountain areas to approximately 9 °C at the basin outlet (Sun et al., 2012).

2. Melt and storm water are the main sources of streamflow. Snow and glacier melt water can account for approximately 63 % of the annual runoff (Shen et al., 2003). Storm water is second to melt water in importance; it mainly occurs during the wet period (May to September) (Xie et al., 2004). Groundwater baseflow is relatively smaller in the wet period but dominates the streamflow in the winter (January, February and December), when both rainfall and melt rarely occur (Kang et al., 1980).

3. The river system of the TRB is a simple fan system. Given the large topography drop and moderate drainage area, runoff concentration time is as short as approximately one day (Xie et al., 2004). Melt and storm water can quickly flow into the main channel and reach the basin outlet.

2.2 Data and preprocessing

A digital elevation model (DEM) from Shuttle Radar Topographic Mission (SRTM) with a spatial resolution of 30 m is used to describe the basin terrain characteristics. A hydrological gauging station, Tailan station (THS, 1602 m a.s.l.), was set up at the basin outlet in 1957. Streamflow, precipitation and temperature series measured on this site are provided by the Aksu Hydrological Bureau. To collect temperature and precipitation data in higher mountainous areas, two automatic weather stations (AWS, product type TRM-ZS2) were set up in June 2011 (i.e. XT AWS, at 2116 m a.s.l. and TG AWS, at 2381 m a.s.l.). The gauged time series data are used to estimate the lapse rate of precipitation and temperature (see below for details). Additionally, the BingTan automatic weather station (BT AWS, at 3950 m a.s.l.) located in the adjacent catchment (Kumalak basin) was used to validate the estimated temperature lapse rates. MODIS remotely sensing snow cover products (SCA) were used to describe the dynamic of snow coverage in TRB, and the China Glacier Inventory (CGI) (Shi, 2008) was used to derive

glacier coverage. To the authors' understanding, most snow would melt off during the warm summer and thus the lowest snow/ice coverage in summer season could be considered to represent the glacier coverage. Based on the analysis of filtered MODIS SCA (see Sect. 2.2.3), the lowest values of snow/ice coverage in summer in the study period (2003–2012) are almost the same, which indicates that glacier coverage is relatively stable during the study period. The DEM, river system, gauging stations and glacier distribution are shown in Fig. 1.

2.2.1 Temperature lapse rate

Altitudinal distribution of temperature can be estimated through the lapse rate (Rango and Martinec, 1979; Tabony, 1985). According to Aizen et al. (2000), rates of temperature decreases with increased elevation are quite different in various months, and ignoring this difference may lead to significant errors in the simulation of snow accumulation and melt. The lapse rate is thus estimated monthly in this study. Temperature value at high altitude can be estimated by the following equation, i.e.:

$$T = T_o + T_p \cdot (H - h) \quad (1)$$

where T_o is the temperature value at low altitude, and T_p is the temperature lapse rate, H and h are the elevation values at high and low positions, respectively, i.e. the mean elevation of two AWS and the elevation of THS here. To obtain the T_p values in different months, the objective function is set as follows:

$$Z = \mathrm{Min}\left[\sum (T_i - (T_{oi} + T_p \cdot (H - h)))\right] \quad (2)$$

where i indicates the ith day in the analyzed month and T_i is the observed value in AWS, which was the mean value of the TG AWS and XT AWS in this study. The estimated monthly lapse rate is presented in Table 1.

To validate the estimated temperature lapse rates, a comparison of estimated temperature and observed temperature in BT AWS is presented in Fig. 2. We also compare the estimated temperature with that estimated by an annual constant lapse rate

($-0.62\,^{\circ}\mathrm{C}\,100\,\mathrm{m}^{-1}$, a similar value to previous studies – Tabony, 1985; Tahir et al., 2011), which is computed by the optimization method above using annual mean temperature. The results show that the temperature produced by monthly lapse rate matched the observed temperature much better than that produced by the annual lapse rate, especially in the summer. The good fit indicates that the temperature at high altitudes can be estimated properly by the monthly temperature lapse rates in Table 1.

2.2.2 Precipitation lapse rate

Based on the precipitation series measured at THS, the monthly precipitation to annual precipitation ratio for the study period (2003–2012) is calculated in Fig. 3, which shows that precipitation varies among months and mainly occurs in May to September and minimally in October to April. The lapse rate of precipitation is also estimated monthly, and a similar procedure for temperature is applied. It should be noted that for precipitation analysis we use a weekly time step instead of a daily time step for temperature and the maximum measured precipitation of the two installed AWS instead of the mean value used for temperature. The analyzed period is limited to the wet period (May to September). Other months are not included due to the relatively smaller quantity of precipitation. The weekly precipitation lapse rates are listed in Table 2. The daily precipitation difference between higher and lower altitudes can be estimated as the weekly precipitation lapse multiplied by the ratio of daily precipitation to the corresponding weekly precipitation in THS. The precipitation lapse rate is not validated by BT AWS because of the significant difference in precipitation distribution features in the two basins (i.e. TRB and Kumalak).

2.2.3 Filtering of MODIS SCA products

Snow cover extent was obtained from MODIS snow cover area (SCA) products. The MOD10A2 and MYD10A2 products having an eight-day time resolution and a 500 m size of cell were used in this study, and were downloaded from the website http:

//reverb.echo.nasa.gov. In total, we obtained 460 eight-day images (two data tiles (i.e. h23v04 and h24v04)) from 2003 to 2012. Daily SCA was interpolation from the eight-day products. However, the accuracy of MODIS SCA product is affected by cloud coverage to a significant degree. Before using the MODIS SCA data as the model input, the remotely sensed images should be filtered to avoid the noise from clouds (Ackerman et al., 1998). The following three successive steps are adopted to filter the products based on previous reports (Gafurov and Bardossy, 2009; Wang et al., 2009; Lopez-Burgos et al., 2012).

Satellite combination: the snow cover products of two satellites, Terra (MOD10A2) and Aqua (MYD10A2) was combined. As long as the value of a pixel is marked as snow in either satellite, the pixel value is marked as snow.

Spatial combination: inspecting the values of the nearest four pixels around one center pixel marked as cloud, if at least three of the four surrounding pixels are marked as snow, the center pixel is modified to be snow.

Temporal combination: if one pixel is marked as cloud, its values in the previous and following observations are investigated. If both of the two observed values are snow, then the present value of the same pixel is snow.

For example, the filtered results from 2004–2005 are shown in Fig. 4, which presents a significant reduction of the fluctuation of SCA products. Furthermore, the lowest values of snow/ice coverage in all years (2003–2012) are similar (from 2003 to 2012 are: 35, 34, 39, 36, 37, 34, 41, 35, 38, 39 %) and close to 33 %, which equals to the value of glacier coverage area in the CGI data mentioned in Sect. 2.1. And MODIS snow/ice cove area in summer is mainly composed of glacier coverage and generally the lowest of the year, when snow has been melt away completely. The filtered results show the relatively stable coverage of glacier.

2.2.4 Spatiotemporal distribution of melt area

The daily temperature in each snow/glacier-covered cell can be estimated by a temperature lapse rate based on the elevation and daily temperature measured at THS. As

long as the temperature exceeded a specific threshold value for melt (simply assumed as 0 °C in this study), a given cell can be labeled as an active cell. The land cover type (glacier, snow or other land cover) for each active cell is estimated by the CGI and MODIS SCA products. The snow alone cover area is calculated by subtracting the glacier area given by CGI from the SCA (a similar procedure can be found in Luo et al., 2013). If a glacier or snow cover cell is active, it is labeled as a melt cell, and the melt area is computed as the number of cells multiplied by the area of each cell.

Organizing the melt area by elevation from low to high and summing the melt area at each elevation each month, the monthly spatial distribution of melt area was obtained. The cumulative melt area in each month (from 2003–2012) and its distribution by elevation is shown in Fig. 5a–b, which shows that melt mainly occurs in May to September. Snowmelt starts at an elevation of approximately 1650 m a.s.l., while glacier melt starts at an elevation of approximately 2950 m a.s.l.

3 Methodology

Runoff generation mechanisms in TRB mainly consist of glacier/snow melt, storm-runoff and groundwater baseflow, and the spatiotemporal variability of hydrometeorological properties (precipitation, temperature and snow/glacier coverage dynamic) can be used to determine the dominant runoff processes for each day. The hydrograph can be further partitioned into several parts according to the dominant mechanisms on a given day, i.e. some parts of the hydrograph may be dominated by groundwater baseflow, some parts by groundwater baseflow and snowmelt processes, some parts by combined glacier and snowmelt processes and groundwater baseflow, and the remainder by a mixture of all processes. Model parameters representing each of these runoff generation mechanisms were grouped, and each group was calibrated separately in a stepwise fashion for the corresponding hydrograph partition. We used the THREW model coupled with a temperature-index model. The initial values of the model

parameters were specified a priori, and only the parameters with significant sensitivity were subject to calibration.

3.1 Partitioning hydrograph

In alpine areas, the relative contributions of different runoff components to the total runoff vary throughout the year (Martinec et al., 1982; Dunn and Colohan, 1999; Yang et al., 2007). Figure 3 shows that precipitation in the TRB varies significantly throughout the year and is primarily concentrated (more than 76 %) in May to September. From October to April, the annual mean rainfall is just 43 mm. Besides, precipitation in the higher mountainous region is mainly snowfall during this period; thus, little runoff is generated by rainfall.

Figure 5 shows that the areas experiencing glacier and snowmelt vary with elevation. Glacier and snowmelt begins at a different elevation each month (minimum elevation of 2950 m and 1650 m, respectively), and snowmelt generally occurs at lower elevations than glacier melt. Because the temperature decreases with increasing elevation, there should exist a period of time during which snowmelt occurs but glacier melt does not. If this occurs between October and April, streamflow will be dominated by snowmelt and groundwater baseflow only.

Based on this physical understanding, we can partition the hydrograph using the following three indices:

1. Date index (DI): DI is used to distinguish the dates on which the storm-runoff process occurs:

$$\mathrm{DI} = \begin{cases} 1, & \text{if the date is between May to September} \\ 0, & \text{if not} \end{cases}. \tag{3}$$

2. Snowmelt index (SI): SI evaluates whether snowmelt occurs on a given day:

$$\mathrm{SI} = \begin{cases} 1, & \text{if the daily temperature at altitude 1650 m is higher than 0 °C} \\ 0, & \text{if not} \end{cases}. \tag{4}$$

3. Glacier melt index (GI): GI is used to identify days when glacier melt occurs:

$$\mathrm{GI} = \begin{cases} 1, & \text{if the daily temperature at altitude 2950 m is higher than 0 °C} \\ 0, & \text{if not} \end{cases}. \tag{5}$$

The hydrograph is then partitioned according to the three indexes as follows:

$$\text{Hydrograph dominated by} \begin{cases} \mathrm{SF} & \text{if SI + GI + DI = 0} \\ \mathrm{SM} & \text{if SI – GI = 1 and DI = 0} \\ \mathrm{SM + GM} & \text{if GI = 1 and DI = 0} \\ \mathrm{SM + GM + } R & \text{if DI = 1} \end{cases} \tag{6}$$

where SF represents groundwater baseflow, SM stands for snowmelt and groundwater baseflow, GM stands for glacier melt, and R represents storm-runoff. The three indexes on each day are calculated, and the streamflow hydrograph is partitioned into four parts according to Eq. (6). Groundwater baseflow is dominant (SF) when melt and direct storm-runoff do not occur (SI + GI + DI = 0); snowmelt and baseflow are dominant (SM) when the temperature at 1650 m a.s.l. is higher than 0 °C and lower than 0 °C at 2950 m a.s.l. (SI – GI = 1 and DI = 0); snow and glacier melt coupled with baseflow dominate (SM + GM) on days when the temperature at 2950 m a.s.l. exceeds 0 °C in October to April (GI = 1 and DI = 0); and finally, all sources are equivalent (SM + GM + R) in the wet period (May to September, DI = 1). Each category contains days that could be continuous or discontinuous in time and could even lie in different weeks due to temporal variability of precipitation and temperature.

3.2 Hydrological model

The Tsinghua Representative Elementary Watershed model (THREW model) is used for the hydrological simulation. The THREW model has been successfully applied in many watersheds in China and the United States (see Tian et al., 2008, 2012; Li et al., 2012; Liu et al., 2012 etc.), which includes an application to a high mountainous catchment of Urumqi River basin by Mou et al. (2008). The THREW model adopts the REW (Representative Elementary Watershed) approach to conceptualize a watershed, originally outlined by Reggiani et al. (1998, 1999), where REW is the elementary unit for hydrological modeling. The whole basin was divided into several REWs based on basin digital elevation model, and each REW is actually a sub-watershed (Tian et al., 2006). REWs are further divided into surface and sub-surface layer, each layer contains several sub-zones. Sub-surface layer is composed of two zones: saturated zone and unsaturated zone, and surface layer consists of six zones: vegetated zone, bare soil zone, snow covered zone, glacier covered zone, sub-stream-network zone, and main channel reach. Further described of these sub-zones can be seen in Tian et al. (2006).

The main runoff generation processes in this study simulated by THREW model is rainfall storm-runoff, snow melt and glacier melt. The proposed hydrograph partition method is based on the relative dominance of these runoff generation mechanisms over time. Storm-runoff is simulated by a Xinanjiang module, which adopts a water storage capacity curve to describe non-uniform distribution of water storage capacity of a REW (Zhao, 1992). The storage capacity curve is determined by two parameters (spatial averaged storage capacity WM and shape coefficient B). Storm-runoff forms on areas where storage is replete. The replete areas are calculated by the antecedent storage and current rainfall. The saturation excess runoff is computed based on water balance.

Precipitation in snow and glacier zone is divided into rainfall and snowfall according to two threshold temperature values (0 and 2.5 °C are adopted in this study according to Wu and Li, 2007), i.e. when temperature is higher than 2.5 °C, all precipitation is

rainfall, when temperature is lower than 0 °C, all precipitation is snowfall, and when temperature falls between the two thresholds, precipitation is divided into rainfall and snowfall in half.

Due to limited available climate data, the THREW model from Mou al. (2008) was modified to couple with the temperature-index method for snow and glacier melt in this study, given the easy accessibility of air temperature data and generally good model performance of the temperature-index model (Hock, 2003). Snow and glacier melt are simulated by a temperature-index model based on degree day factors (Eq. 7):

$$M = \mathrm{DDF} \cdot \omega \cdot (T_\mathrm{t} - T_\mathrm{o}) \quad (7)$$

where M (mm) is the amount of ice or snow melt, DDF is degree-day factor expressed in $\mathrm{mm\,d^{-1}\,^\circ C^{-1}}$, T_t (°C) is daily mean temperature, and T_o (°C) is a threshold temperature beyond which melt occurs. ω is the snow or glacier cover area fraction in the REW. The melt model needs daily temperature and the area of the glacier and snow cover zone in each REW to run. Snow cover areas were updated by MODIS SCA data, and glacier area was described as glacier coverage in CGI, which is remain stable during the study period (2003–2012). Both storm-runoff and melt flow into the sub-stream-network and are routed along the channel by Saint-Venant equations to the basin outlet.

3.3 Stepwise calibration

Model parameters were first grouped according to their connection with the causal physical mechanisms, following which the relative impact of each parameter group on basin hydrograph was analyzed (see Sect. 3.4 for details). Only a few key (significantly sensitive) parameters that control the snowmelt, glacier melt, and storm-runoff runoff generation mechanisms were selected for calibration. These parameters are related to the corresponding hydrograph parts and then calibrated stepwise, as follows: (a) groundwater baseflow was separated from the total hydrograph via an automatic filtering procedure developed by Arnold et al. (1995, 1999), (b) the snowmelt degree day factor (SDDF) was calibrated on days in the SM component of the hydrograph,

(c) the glacier melt degree day factor (GDDF) was calibrated on days in the SM + GM component of the hydrograph, (d) storm-runoff parameters (B, WM) were calibrated on DI = 1 days, i.e. the SM + GM + R component of the hydrograph.

The Nash-Sutcliffe coefficient (NS) was used as an evaluation criterion for each calibration step. Each parameter group was calibrated separately and then kept constant in the following steps. Because MODIS (i.e. MYD10A2) began to provide whole year data in 2003, the simulation period is from 2003 to 2012, in which 2003–2007 is the calibration period, and 2008–2012 is the validation period.

Because the simulation in each step can, to some degree, be affected by the initial conditions produced in the preceding step, repeated iteration was implemented to reduce this influence. The parameters were first calibrated based on their individual hydrograph parts according to an optimal NS value, and then the sequence of steps in the above paragraph was repeated several times until the optimized parameters no longer changed.

3.4 A priori determination of model parameters

The parameters for the hydrological model are grouped in Table 3. According to Xie et al. (2004) and Kang et al. (1980), snow and glacier melt contribute approximately 63 % to the total annual runoff in TRB, and melt water and storm-runoff dominate the streamflow in the wet period (May to September), which accounts for approximately 80 % of the total annual runoff. The parameters, i.e. SDDF, GDDF, WM and B, in the melt and storm-runoff group should be significantly sensitive to the hydrograph simulation. The effects of other parameter groups are analyzed as follows.

- Subsurface: in this study, groundwater baseflow is separated from the hydrograph by an automatic procedure. The parameters in subsurface group have a small effect on model simulation due to the low ratio of baseflow to the total streamflow volume (approximately 18 %, consistent with Kang et al., 1980).

- Infiltration: on the daily time scale, average rainfall intensity is too low to generate infiltration excess runoff in TRB, and therefore all surface runoff is assumed to be saturation excess runoff in our model. Additionally, groundwater recharged by infiltration is low, which indicates that infiltration has a minimal influence on stream discharge.

- Interception: to investigate the interception effect on TRB runoff, remotely sensed land cover data were drawn from MODIS (MCD12Q1) in Fig. 6, which shows that woody plant coverage is low in the TRB. The influence of interception on basin runoff should be limited.

- Evaporation: according to Shen et al. (2003), evaporation has a significant effect on local water balance and accounts for approximately 10 % of the total runoff. The value of the evaporation parameter, k_v, in this study is the same as that used by Sun et al. (2012). The calibration of this parameter by the same procedure used for the runoff generation parameters should be explored but has been left for future research.

- Routing: according to Xie et al. (2004), melt and storm water can flow quickly into the main channel and arrive at the basin outlet within one day. The hydrograph simulation is insensitive to routing parameters, which was decided a priori based on Gao et al. (2011) and Xie et al. (2004).

The above low-impact parameters are determined a priori according to Sun et al. (2012) and are shown in Table 3. To facilitate the illustration of our diagnostic approach, only the calibration of the four key parameters (SDDF, GDDF, WM, and B) is implemented. The initial values for the four parameters are also determined a priori as 2.8 mm °C^{-1} day^{-1} for SDDF, 4.3 mm °C^{-1} day^{-1} for GDDF, 0.35 m for WM and 0.33 for B, which are all based on Sun et al. (2012) and Tian et al. (2012).

4 Results and discussion

4.1 Partitioned hydrograph

The hydrograph for 2003–2007 was partitioned based on Eq. (6). As an example, the partitioned results for 2003 are shown in Fig. 7. The figure shows that the melt period in 2003 ranged from early March to late November (indicated by red dots, green dots and blue dots), during which snowmelt occurred continually, while glacier melt started later and stopped earlier (green dots and blue dots), in agreement with previous studies of Sun et al. (2012) and Kang et al. (1980). Hydrograph sections dominated by groundwater baseflow mainly fell into December, January and February and are denoted by black dots, while storm-runoff occurred only in the wet period (May to September, denoted by blue dots).

The total number of SM days from 2003 to 2007 was 365, and there were 249 SM+GM days, while SM+GM+R accounted for 765 days. The number of days when no melt occurred from 2003 to 2007 was 114, 80, 89, 96, and 68. The mean temperatures in those years gauged at the THS were 8.9, 10.1, 9.9, 10.4, 11.3 °C. Years have lower mean temperatures have longer no-melt days and vice versa. The partition results provide 365 daily streamflow (discontinuous) for calibration of SDDF, 249 daily streamflow (discontinuous) for GDDF and 765 daily streamflow (discontinuous) for calibration of WM and B.

4.2 Parameter calibration

The four key parameters (SDDF, GDDF, WM, and B) were separately calibrated using individual hydrograph partitions in a stepwise way, and an iterative calibration approach was adopted to minimize the interaction between steps. A total of 18 iterations were implemented, and the simulation of the first three iterations and the last iteration are shown in Fig. 8. From the first iteration to the last iteration, the correspondence between the simulations and observations increased, especially for high flows. The simulations

in each step of the last iteration are presented in Fig. 9. Figure 9a demonstrates that winter streamflow was dominated by groundwater baseflow in the TRB, while in other months, especially in the wet period, the total runoff was much higher than groundwater baseflow, indicating that other runoff generation mechanisms occurred. In the SM part in Fig. 9b, streamflow was dominated by both snowmelt and groundwater baseflow. The SDDF parameter was determined according to the remaining discharge difference in this section after the separation of groundwater baseflow. The calibrated SDDF is 0.9 mm °C^{-1} day^{-1} (Table 4) with an optimized NS value of −0.49. Although the NS value is relatively low due to inadequate estimation of groundwater baseflow, the main peak flows caused by temperature increases were captured well. For the SM + GM part, glacier melt began to control the streamflow in combination with snowmelt and groundwater baseflow. Both snowmelt and baseflow can be calculated a priori. The remaining residual between the simulation and observation discharge can be attributed to glacier melt alone and used for calibration of the glacier melt factor GDDF. The NS value for this step had risen to 0.26 and we obtained a sound simulation of peak flows with a calibrated GDDF of 9.0 mm °C^{-1} day^{-1} (Table 4), a value similar to that reported in other studies (Singh et al., 2000). In wet periods (SM + GM + R), melt alone cannot completely describe the runoff, because storm-runoff is an important component of basin runoff. The parameters WM and B for storm-runoff were calibrated with the help of calculated melt factors (SDDF and GDDF) and groundwater baseflow individually. The NS value in this period is 0.46, with WM = 0.6 m and B = 0.8 (Table 4). Main peak flows were captured well, with a good match to the trend and magnitude of the total hydrograph (Fig. 9d). The entire daily simulation is shown in Fig. 10a and has an NS value of 0.79, which indicates sound performance of the model. The simulated proportions of snow and glacier melt to total runoff in 2003 to 2007 is 59.2 % (6.1 % snow and 53.1 % glacier), which is similar to the 7.4 % snow, 57.6 % glacier and 65 % combined proportions reported by Kang et al. (1980) and Sun et al. (2012). The results indicate that the parameters calibrated independently in each step can lead to a good

overall simulation except for some large summer peak events, which could be caused by heavy storm events but were not properly monitored by rain gauge equipment.

To validate the stability of the calibrated parameters, the calibrated parameter set was used in a validation period from 2008 to 2012. The hydrograph in this period was partitioned based on dominant runoff generation mechanisms, as was done for the calibration years 2003–2007 (Fig. 10b). The simulated discharge did not match the observed value as well as in the calibrated period as indicated by the NS value of 0.61 for this five-year period (Fig. 10b). The lower performance mainly occurred on storm-runoff days (SM + GM + R) (NS value of 0.23), especially for some extreme storm events in the summer of 2010. Again, the underestimation of these events is likely due to inadequate observations of rainfall, which are principally due to the strong spatial variability of rainfall in mountainous areas. Generally, we can say that (a) the parameter set calibrated in a stepwise way can produce a relatively stable simulation for both the calibration and validation periods, and (b) the model simulation is affected by some types of uncertainty, e.g. the uncertainty in the estimation of rainfall data.

4.3 Comparison with automatic calibration method

We also calibrated the model automatically with the help of the ε-NSGAII algorithm, an optimization method developed by Deb et al. (2002) and Kollat and Reed (2006). The four parameters calibrated automatically are shown in Table 4. The values are similar to those calibrated by the hydrograph partition method, indicating that the partitioned method is comparable to an automatic method. However, it should be noted that the CPU time consumption by the automatic method for this task is about one month (Intel Core i7 CPU and 2.8 GHz), whereas the partitioned method just took about 8 h. Table 5 shows the comparison of NS values for every hydrograph part. The results suggest general agreement between the two methods, although the automatic method has lower NS values especially for the SM and SM + GM parts. According to Kuczera and Mroczkowski (1998), models with more than four or five parameters calibrated to streamflow data often have poor parameter identifiability. Additionally, several studies

have suggested that the ratio between the number of parameters and number of criteria handled by an automatic calibration procedure should be lower than 5 : 1 (Beven, 1989; Jakeman and Hornberger, 1993; Gupta, 2000). In this study, the number of calibrated parameter is four, and number of criteria is one, so automatic method can properly identify these parameters. However, when the calibrated parameter dimension increases to more than four, the automatic method may become less successful by ignoring the physical basis of each parameter, while this would not impact the partitioned method because each parameter is calibrated in an individual process. Also, the automatic method can be sensitive to calibration data (Yapo et al., 1996), which means that different calibration data can produce different parameter sets. In regard to the partitioned method, parameters are determined by individual hydrograph parts, which could avoid the selection issue for the calibration data set.

4.4 Cross validation

To test the robustness of the partitioned calibration method, cross validation was performed. We calibrated the model for 2008–2012 and validated the parameters for 2003–2007. The new calibrated parameter set is SDDF = 0.8 mm °C^{-1} day^{-1}, GDDF = 9.0 mm °C^{-1} day^{-1}, WM = 0.7 m and B = 0.2, which is very similar to the calibrated values in 2003–2007 listed in Table 4. The NS values for 2008–2012 and 2003–2007 simulated by this parameter set are 0.62 and 0.77, respectively. The most obvious difference is the value of parameter B (0.2 to 0.8), which may be attributed to the difference in peak flow magnitudes in the summers of the two periods, as shown in Fig. 10. The simulations of the two periods by cross validation are presented in Fig. 11, which shows reasonably good performance during both periods, further demonstrating the robustness of the proposed partitioned calibration method.

5 Summary and conclusion

This study proposed an approach to extract information from available data series in an alpine area, which can be further used to partition hydrographs pertaining to dominant runoff generation mechanisms. The parameters of a hydrological model were grouped, related to individual hydrograph partitions and separately calibrated by their physical processes in a stepwise way, which means that the calibrated parameters are fixed as constants in the following procedures. An application of the model to an alpine watershed in the Tianshan Mountains in northwestern China showed that the method performed reasonably well, even with very limited gauged climate data. Cross validation and comparison to an automatic calibration method indicated its robustness, while the low performance of the model for extreme summer storm events indicated the inadequacy of rainfall measurement.

To be noted, a simplified semi-distributed hydrological model was used to facilitate the illustration of proposed diagnostic calibration approach in the high mountainous Tailan River basin. The glacier mass balance is not simulated in the model and the glacier coverage is fixed during the study period, which could be subject to significant change in the context of global warming. According to existing studies (Stahl et al., 2008; Schaefli and Huss, 2011; Jost et al., 2012), glacier mass balance data is useful to constrain the parameter uncertainty for hydrological modeling in a glaciered basin. While arguing that our assumption of unchanged glacier coverage will not weaken the importance of the proposed approach, we acknowledge that the improved model coupled with glacier mass balance equations will improve the accuracy of hydrological simulation aided by glacier mass balance observations. This is left for future research.

A prerequisite for the proposed approach is hydrograph partitioning based on dominant runoff generation mechanisms. The key to the partition procedure is to identify the functional domain of each runoff generation mechanism from signature information extracted from easily available data. A partition can be achieved in which the relative roles of different runoff components in the basin runoff vary significantly with time. The

alpine watershed is a typical area in which the dominant mechanisms can be separated by the combination of topography, ground-gauged temperature and precipitation, and remotely sensed snow and glacier coverage. Other areas with strong temporal variability of catchment wetness along with precipitation (e.g. monsoon zones) could also be suitable for the proposed approach. The Dunne runoff is prone to dominate the hydrograph when the catchment is wet and it could switch to Hortonian runoff rapidly under the combination of high evaporative demand and less precipitation, as shown by Tian et al. (2012) in the Blue River basin of Oklahoma. This is, however, also left for future research.

Acknowledgements. We wish to thank Wang Xinhui for his assistance in collecting hydrometeorology data in the Tailan River basin, and thank Charlie Luce and Viviana Lopez-Burgos who provided great help in MODIS product filtering. The authors would also like to thank sincerely Editor Markus Weiler for his careful comments which improve the quality of manuscript significantly. This study was supported by the National Science Foundation of China (NSFC 51190092, U1202232, 51222901) and the foundation of the State Key Laboratory of Hydroscience and Engineering of Tsinghua University (2012-KY-03). Their supports are greatly appreciated.

References

Ackerman, S. A., Strabala, K. I., Menzel, W. P., Frey, R. A., Moeller, C. C., and Gumley, L. E.: Discriminating clear sky from clouds with MODIS, J. Geophys. Res., 103, 32141–32157, 1998.

Aizen, V., Aizen, E., Glazirin, G., and Loaiciga, H. A.: Simulation of daily runoff in Central Asian alpine watersheds, J. Hydrol., 238, 15–34, 2000.

Arnold, J. G. and Allen, P. M.: Automated methods for estimating baseflow and ground water recharge from streamflow records, J. Am. Water Resour. Assoc., 35, 411–424, 1999.

Arnold, J. G., Allen, P. M., Muttiah, R., and Bernhardt, G.: Automated base-flow separation and recession analysis techniques, Ground Water, 33, 1010–1018, 1995.

Beven, K.: Changing ideas in hydrology – the case of physically-based models, J. Hydrol., 105, 157–172, 1989.

Beven, K.: Prophecy, reality and uncertainty in distributed hydrological modelling, Adv. Water Resour., 16, 41–51, 1993.
Beven, K.: Equifinality and uncertainty in geomorphological modelling, in: The Scientific Nature of Geomorphology: Proceedings of the 27th Binghamton Symposium in Geomorphology, Chichester, 289–313, 1996.
Beven, K. and Binley, A.: The future of distributed models-model calibration and uncertainty prediction, Hydrol. Process., 6, 279–298, 1992.
Beven, K. and Freer, J.: Equifinality, data assimilation, and uncertainty estimation in mechanistic modelling of complex environmental systems using the GLUE methodology, J. Hydrol., 249, 11–29, 2001.
Boyle, D. P., Gupta, H. V., and Sorooshian, S.: Toward improved calibration of hydrologic models: combining the strengths of manual and automatic methods, Water Resour. Res., 36, 3663–3674, 2000.
Brazil, L.: Multilevel calibration strategy for complex hydrologic simulation models, NOAA Technical Report, NWS 42, Fort Collins, 217 pp., 1989.
Deb, K., Pratap, A., Agarwal, S., and Meyarivan, T.: A fast and elitist multiobjective genetic algorithm: NSGA-II, IEEE T. Evolut. Comput., 6, 182–197, 2002.
Detenbeck, N. E., Brady, V. J., Taylor, D. L., Snarski, V. M., and Batterman, S. L.: Relationship of stream flow regime in the western Lake Superior basin to watershed type characteristics, J. Hydrol., 309, 258–276, 2005.
Duan, Q., Sorooshian, S., and Gupta, V.: Effective and efficient global optimization for conceptual rainfall-runoff models, Water Resour. Res., 28, 1015–1031, 1992.
Dunn, S. M. and Colohan, R. J. E.: Developing the snow component of a distributed hydrological model: a step-wise approach based on multi-objective analysis, J. Hydrol., 223, 1–16, 1999.
Eder, G., Fuchs, M., Nachtnebel, H., and Loibl, W.: Semi-distributed modelling of the monthly water balance in an alpine catchment, Hydrol. Process., 19, 2339–2360, 2005.
Farmer, D., Sivapalan, M., and Jothityangkoon, C.: Climate, soil, and vegetation controls upon the variability of water balance in temperate and semiarid landscapes: downward approach to water balance analysis, Water Resour. Res., 39, 1035, doi:10.1029/2001WR000328, 2003.
Gafurov, A. and Bárdossy, A.: Cloud removal methodology from MODIS snow cover product, Hydrol. Earth Syst. Sci., 13, 1361–1373, doi:10.5194/hess-13-1361-2009, 2009.

Gan, T. Y. and Biftu, G. F.: Automatic calibration of conceptual rainfall-runoff models: Optimization algorithms, catchment conditions, and model structure, Water Resour. Res., 32, 3513–3524, 1996.
Gao, W., Li, Z., and Zhang, M.: Study on Particle-size Properties of Suspended Load in Glacier Runoff from the Tomor Peak, Arid Zone Res., 28, 449–454, 2011.
Gomez-Landesa, E. and Rango, A.: Operational snowmelt runoff forecasting in the Spanish Pyrenees using the snowmelt runoff model, Hydrol. Process., 16, 1583–1591, 2002.
Gupta, H. V.: Penman Lecture, in: 7th BHS National Symposium, Newcastle-upon-Tyne, UK, 2000.
Gupta, H. V., Sorooshian, S., and Yapo, P. O.: Toward improved calibration of hydrologic models: multiple and noncommensurable measures of information, Water Resour. Res., 34, 751–763, 1998.
Gupta, H. V., Wagener, T., and Liu, Y.: Reconciling theory with observations: elements of a diagnostic approach to model evaluation, Hydrol. Process., 22, 3802–3813, 2008.
Gupta, H. V., Kling, H., Yilmaz, K. K., and Martinez, G. F.: Decomposition of the mean squared error and NSE performance criteria: Implications for improving hydrological modelling, J. Hydrol., 377, 80–91, 2009.
Gupta, V. K. and Sorooshian, S.: Uniqueness and observability of conceptual rainfall-runoff model parameters: the percolation process examined, Water Resour. Res., 19, 269–276, 1983.
Gupta, V. K. and Sorooshian, S.: The automatic calibration of conceptual catchment models using derivative-based optimization algorithms, Water Resour. Res., 21, 437–485, 1985.
Gurtz, J., Baltensweiler, A., and Lang, H.: Spatially distributed hydrotope-based modelling of evapotranspiration and runoff in mountainous basins, Hydrol. Process., 13, 2751–2768, 1999.
Haberlandt, U., Klocking, B., Krysanova, V., and Becker, A.: Regionalisation of the base flow index from dynamically simulated flow components – a case study in the Elbe River Basin, J. Hydrol., 248, 35–53, 2001.
Hock, R.: Temperature index melt modelling in mountain areas, J. Hydrol., 282, 104–115, 2003.
Hooper, R. P. and Shoemaker, C. A.: A Comparison of Chemical and Isotopic Hydrograph Separation, Water Resour. Res., 22, 1444–1454, 1986.
Jakeman, A. J. and Hornberger, G. M.: How much complexity is warranted in a rainfall-runoff model?, Water Resour. Res., 29, 2637–2649, 1993.

Johnston, P. R. and Pilgrim, D. H.: Parameter optimization for watershed models, Water Resour. Res., 12, 477–486, 1976.
Jost, G., Moore, R. D., Menounos, B., and Wheate, R.: Quantifying the contribution of glacier runoff to streamflow in the upper Columbia River Basin, Canada, Hydrol. Earth Syst. Sci., 16, 849–860, doi:10.5194/hess-16-849-2012, 2012.
Jothityangkoon, C., Sivapalan, M., and Farmer, D. L.: Process controls of water balance variability in a large semi-arid catchment: downward approach to hydrological model development, J. Hydrol., 254, 174–198, 2001.
Kang, E., Zhu, S., and Huang, M.: Some results of the research on glacial hydrology in the region of MT. Tuomuer, J. Glaciol. Geocryol., 2, 18–21, 1980.
Kollat, J. B. and Reed, P. M.: Comparing state-of-the-art evolutionary multi-objective algorithms for long-term groundwater monitoring design, Adv. Water Resour., 29, 792–807, 2006.
Konz, M. and Seibert, J.: On the value of glacier mass balances for hydrological model calibration, J. Hydrol., 385, 238–246, 2010.
Kuczera, G. and Mroczkowski, M.: Assessment of hydrologic parameter uncertainty and the worth of multiresponse data, Water Resour. Res., 34, 1481–1489, 1998.
Li, H. Y., Sivapalan, M., and Tian, F. Q.: Comparative diagnostic analysis of runoff generation processes in Oklahoma DMIP2 basins: the Blue River and the Illinois River, J. Hydrol., 418, 90–109, 2012.
Liu, D. F., Tian, F. Q., Hu, H. C., and Hu, H. P.: The role of run-on for overland flow and the characteristics of runoff generation in the Loess Plateau, China, Hydrolog. Sci. J., 57, 1107–1117, 2012.
López-Burgos, V., Gupta, H. V., and Clark, M.: A probability of snow approach to removing cloud cover from MODIS Snow Cover Area products, Hydrol. Earth Syst. Sci. Discuss., 9, 13693–13728, doi:10.5194/hessd-9-13693-2012, 2012.
Luo, Y., Arnold, J., Liu, S., Wang, X., and Chen, X.: Inclusion of glacier processes for distributed hydrological modeling at basin scale with application to a watershed in Tianshan Mountains, northwest China, J. Hydrol., 477, 72–85, 2013.
Martinec, J., Oeschger, H., Schotterer, U., and Siegenthaler, U.: Snowmelt and groundwater storage in alpine basin, in: Hydrological Aspects of Alpine and High Mountain Areas, IAHS Press, Wallingford, UK, 169–175, 1982.
McCuen, R. H.: Hydrologic Analysis and Design, Prentice Hall, New Jersey, 355–360, 1989.

Mendoza, G. F., Steenhuis, T. S., Walter, M. T., and Parlange, J. Y.: Estimating basin-wide hydraulic parameters of a semi-arid mountainous watershed by recession-flow analysis, J. Hydrol., 279, 57–69, 2003.
Mou, L., Tian, F., Hu, H., and Sivapalan, M.: Extension of the Representative Elementary Watershed approach for cold regions: constitutive relationships and an application, Hydrol. Earth Syst. Sci., 12, 565–585, doi:10.5194/hess-12-565-2008, 2008.
Nash, J. E. and Sutcliffe, J. V.: River flow forecasting through conceptual models, part I – A discussion of principles, J. Hydrol., 10, 282–290, 1970.
Nathan, R. J. and McMahon, T. A.: Evaluation of automated techniques for base flow and recession analyses, Water Resour. Res., 26, 1465–1473, 1990.
Nejadhashemi, A. P., Shirmohammadi, A., Sheridan, J. M., Montas, H. J., and Mankin, K. R.: Case study: evaluation of streamflow partitioning methods, J. Irrig. Drain. E.-ASCE, 135, 791–801, 2009.
Pinder, G. F. and Jones, J. F.: Determination of the ground-water component of peak determination of the ground-water component of peak discharge from the chemistry of total runoff, Water Resour. Res., 5, 438–445, 1969.
Rango, A. and Martinec, J.: Application of a snowmelt-runoff model using landsat data, Nord. Hydrol., 10, 225–238, 1979.
Reggiani, P., Sivapalan, M., and Hassanizadeh, S. M.: A unifying framework for watershed thermodynamics: balance equations for mass, momentum, energy and entropy, and the second law of thermodynamics, Adv. Water Resour., 22, 367–398, 1998.
Reggiani, P., Hassanizadeh, S. M., Sivapalan, M., and Gray, W. G.: A unifying framework for watershed thermodynamics: constitutive relationships, Adv. Water Resour., 23, 15–39, 1999.
Richter, B. D., Baumgartner, J. V., Powell, J., and Braun, D. P.: A method for assessing hydrologic alteration within ecosystems, Conserv. Biol., 10, 1163–1174, 1996.
Schaefli, B. and Huss, M.: Integrating point glacier mass balance observations into hydrologic model identification, Hydrol. Earth Syst. Sci., 15, 1227–1241, doi:10.5194/hess-15-1227-2011, 2011.
Shamir, E., Imam, B., Gupta, H. V., and Sorooshian, S.: Application of temporal streamflow descriptors in hydrologic model parameter estimation, Water Resour. Res., 41, W06021, doi:10.1029/2004WR003409, 2005a.

Shamir, E., Imam, B., Morin, E., Gupta, H. V., and Sorooshian, S.: The role of hydrograph indices in parameter estimation of rainfall-runoff models, Hydrol. Process., 19, 2187–2207, 2005b.
Shen, Y., Liu, S., Ding, Y., and Wang, S.: Glacier Mass Balance Change in Tailanhe River Watersheds on the SouthSlope of the Tianshan Mountains and its impact on water resources, J. Glaciol. Geocryol., 25, 124–129, 2003.
Shi, Y.: Concise Glacier Inventory of China, Shanghai Popular Science Press., Shanghai, China, 2008.
Singh, P., Kumar, N., and Arora, M.: Degree-day factors for snow and ice for Dokriani Glacier, Garhwal Himalayas, J. Hydrol., 235, 1–11, 2000.
Sivapalan, M., Bloschl, G., Zhang, L., and Vertessy, R.: Downward approach to hydrological prediction, Hydrol. Process., 17, 2101–2111, 2003.
Sorooshian, S. and Gupta, V. K.: Automatic calibration of conceptual rainfall-runoff models-the question of parameter observability and uniqueness, Water Resour. Res., 19, 260–268, 1983.
Spear, R. C. and Hornberger, G. M.: Eutrophication in peel inlet – II. Identification of critical uncertainties via generalized sensitivity analysis, Water Resour., 14, 43–49, 1980.
Stahl, K., Moore, R. D., Shea, J. M., Hutchinson, D., and Cannon, A. J.: Coupled modelling of glacier and streamflow response to future climate scenarios, Water Resour. Res., 44, W02422, doi:10.1029/2007WR005956, 2008.
Sun, M., Yao, X., Li, Z., and Li, J.: Estimation of Tailan River discharge in the Tianshan Mountains in the 21st century, Adv. Clim. Change Res., 8, 342–349, 2012.
Tabony, R. C.: The variation of surface temperature with altitude, Meteorol. Mag., 114, 37–48, 1985.
Tahir, A. A., Chevallier, P., Arnaud, Y., Neppel, L., and Ahmad, B.: Modeling snowmelt-runoff under climate scenarios in the Hunza River basin, Karakoram Range, Northern Pakistan, J. Hydrol., 409, 104–117, 2011.
Tian, F. Q., Hu, H., Lei, Z., and Sivapalan, M.: Extension of the Representative Elementary Watershed approach for cold regions via explicit treatment of energy related processes, Hydrol. Earth Syst. Sci., 10, 619–644, doi:10.5194/hess-10-619-2006, 2006.
Tian, F. Q., Hu, H. P., and Lei, Z. D.: Thermodynamic watershed hydrological model: constitutive relationship, Sci. China Ser. E, 51, 1353–1369, 2008.

Tian, F. Q., Li, H. Y., and Sivapalan, M.: Model diagnostic analysis of seasonal switching of runoff generation mechanisms in the Blue River basin, Oklahoma, J. Hydrol., 418, 136–149, 2012.
van Griensven, A. and Bauwens, W.: Multiobjective autocalibration for semidistributed water quality models, Water Resour. Res., 39, 1348, doi:10.1029/2003WR002284, 2003.
Van Straten, G. T. and Keesman, K. J.: Uncertainty propagation and speculation in projective forecasts of environmental change: a lake-eutrophication example, J. Forecasting, 10, 163–190, 1991.
Vivoni, E. R., Entekhabi, D., Bras, R. L., and Ivanov, V. Y.: Controls on runoff generation and scale-dependence in a distributed hydrologic model, Hydrol. Earth Syst. Sci., 11, 1683–1701, doi:10.5194/hess-11-1683-2007, 2007.
Vrugt, J. A., Gupta, H. V., Bastidas, L. A., Bouten, W., and Sorooshian, S.: Effective and efficient algorithm for multiobjective optimization of hydrologic models, Water Resour. Res., 39, 1214, doi:10.1029/2002WR001746, 2003a.
Vrugt, J. A., Gupta, H. V., Bouten, W., and Sorooshian, S.: A shuffled complex evolution metropolis algorithm for optimization and uncertainty assessment of hydrological model parameters, Water Resour. Res., 39, 1201, doi:10.1029/2002WR001642, 2003b.
Wang, X. W., Xie, H. J., Liang, T. G., and Huang, X. D.: Comparison and validation of MODIS standard and new combination of Terra and Aqua snow cover products in northern Xinjiang, China, Hydrol. Process., 23, 419–429, 2009.
Wu, J. and Li, L.: A rain-on-snow mixed flood forecast model and its application, Eng. J. Wuhan Univ., 40, 20–23, 2007.
Xie, C., Ding, Y., Liu, S., and Han, H.: Analysis on the glacial hydrological features of the glaciers on the south slope of Mt. Tuomuer and the effects on runoff, Arid Land Geogr., 27, 570–575, 2004.
Yadav, M., Wagener, T., and Gupta, H.: Regionalization of constraints on expected watershed response behavior for improved predictions in ungauged basins, Adv. Water Resour., 30, 1756–1774, 2007.
Yang, D. Q., Zhao, Y. Y., Armstrong, R., Robinson, D., and Brodzik, M. J.: Streamflow response to seasonal snow cover mass changes over large Siberian watersheds, J. Geophys. Res., 112, F02S22F2, doi:10.1029/2006JF000518, 2007.
Yapo, P. O., Gupta, H. V., and Sorooshian, S.: Automatic calibration of conceptual rainfall-runoff models: sensitivity to calibration data, J. Hydrol., 181, 23–48, 1996.

Yilmaz, K. K., Gupta, H. V., and Wagener, T.: A process-based diagnostic approach to model evaluation: application to the NWS distributed hydrologic model, Water Resour. Res., 44, W09417, doi:10.1029/2007WR006716, 2008.
Zhao, R. J.: The Xinanjiang model applied in China, J. Hydrol., 135, 371–381, 1992.

Table 1. Estimated monthly lapse rate of temperature in the TRB.

Month	Temperature lapse rate ($^{\circ}$C daily^{-1} 100 m^{-1})
Jan	−0.38
Feb	−0.38
Mar	−0.66
Apr	−0.76
May	−0.8
Jun	−0.78
Jul	−0.82
Aug	−0.86
Sep	−0.66
Oct	−0.6
Nov	−0.54
Dec	−0.3
Annual	−0.62

Table 2. Estimated weekly precipitation lapse rate in wet months.

Month	Precipitation lapse rate (mm week^{-1} 100 m^{-1})
May	1.63
Jun	1.69
Jul	3.14
Aug	2.40
Sep	2.28

Table 3. Parameter properties in the THREW model.

Category	Symbol	Unit	Description	Value
Subsurface	K_s^u	m s^{-1}	Saturated hydraulic conductivity for *u* zone	1.25×10^{-05}
	K_s^s	m s^{-1}	Saturated hydraulic conductivity for *s* zone	1.25×10^{-05}
	ε^u	–	Soil porosity value of *u* zone	4.80×10^{-01}
	ε^s	–	Soil porosity value of *s* zone	2.88×10^{-01}
	Ψ_a	m	Air entry value	2.50×10^{-01}
	μ	–	Soil pore size distribution index	2.00×10^{-01}
	KKA	–	Coefficient used to calculate subsurface flow	$1.10 \times 10^{+00}$
	β^k	–	Coefficient used to calculate unsaturated hydraulic conductivity	8.00×10^{-01}
	β^Ψ	–	Coefficient used to calculate matrix potential	2.50×10^{-01}
	α_{vz}^u	–	Spatial heterogeneous coefficient for flow velocity of *u* zone	$1.03 \times 10^{+00}$
	α^{us}	–	Spatial heterogeneous coefficient for flow flux between *u* zone and *s* zone	$1.66 \times 10^{+00}$
	k^b	–	Empirical coefficient used to estimate the potential crack volume of soil layer	$0.00 \times 10^{+00}$
Routing	n^t	–	Manning roughness coefficient for hillslope, obtained from the literature according to land use and vegetation type	1.50×10^{-01}
	n^r	–	Similar to n^t, roughness coefficient for channel	3.00×10^{-01}
	α^{tr}	–	Spatial heterogeneous coefficient for flow flux between *t* zone and *r* zone	1.10×10^{-01}
Infiltration	α^{EFL}	–	Spatial heterogeneous coefficient for exfiltration capacity	$1.00 \times 10^{+00}$
	α^{IFL}	–	Spatial heterogeneous coefficient for infiltration capacity	$1.50 \times 10^{+00}$
Interception	$Fmax^b$	m	Ground surface depression storage capacity	$0.00 \times 10^{+00}$
	α^{vb}	m	Maximum rainfall depth a single leaf can intercept and hold	1.00×10^{-05}
Evaporation	k_v	–	Ratio of potential evapotranspiration over potential evaporation	9.00×10^{-01}
Storm-runoff	*B*	–	Shape coefficient to calculate the saturation excess runoff area from the Xin'anjiang model	Calibrated
	WM	m	Spatial averaged tension water storage capacity in the Xin'anjiang model	Calibrated
Melt	GDDF	mm °C^{-1} day^{-1}	Degree per day factor used to calculate glacier melt in the temperature-index model, which is subject to calibration	Calibrated
	SDDF	mm °C^{-1} day^{-1}	Degree per day factor used to calculate snowmelt in the temperature-index model, which is subject to calibration	Calibrated

Table 4. Calibrated parameter values.

Parameter	Partition calibration	Automatic calibration
GDDF(mm °C^{-1} day^{-1})	9.00	9.07
SDDF(mm °C^{-1} day^{-1})	0.90	0.85
WM(m)	0.60	0.59
B	0.80	0.97

Table 5. Comparison of simulated NS values for each hydrograph part from the automatic and partitioned calibration methods.

Period	Part	Partitioned calibration	Automatic calibration
2003–2007	SM	−0.49	−0.52
	SM + GM	0.26	0.24
	SM + GM + *R*	0.46	0.46
2008–2012	SM	0.70	0.68
	SM + GM	0.21	0.15
	SM + GM + *R*	0.23	0.22

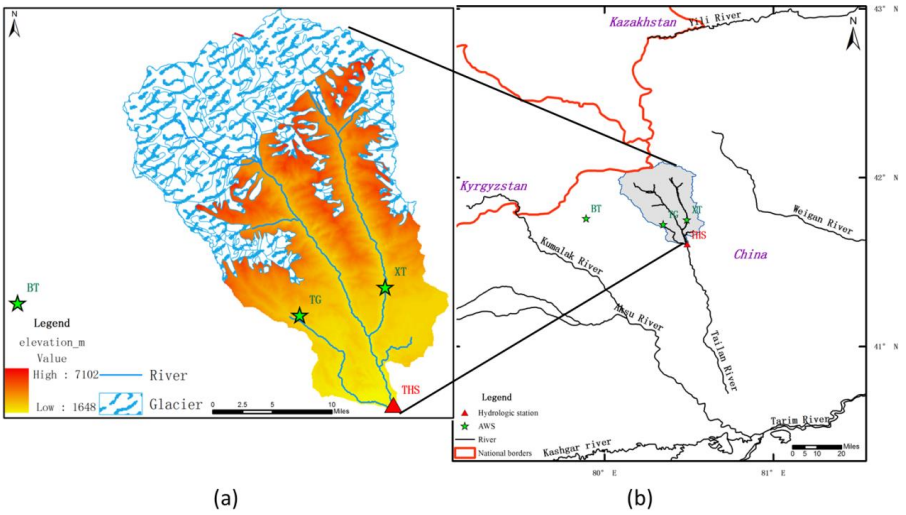

Fig. 1. Location of the Tailan River basin in Xinjiang, China. Two automatic weather stations (TG at 2381 m a.s.l. and XT at 2116 m a.s.l.) were set up in an upstream mountain area in July 2011. Additionally, the BT AWS (at 3950 m a.s.l.) located in the adjacent catchment (Kumalak basin) was used to validate the estimated temperature lapse rates. The Tailan Hydrologic Station (THS) has gauged streamflow data at the catchment outlet since 1957 **(b)**. Glacier coverage occupies approximately 33 % of the total basin area **(a)**.

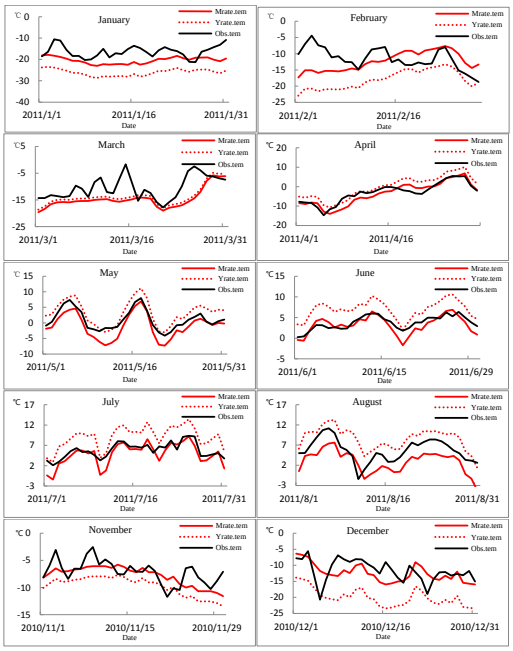

Fig. 2. Validation of the estimated temperature lapse rate at the BT AWS. The black solid line is the observed temperature series at the BT AWS (Obs.tem); the red solid line is the estimated temperature by monthly lapse rate (Mrate.tem). The red dotted line indicates the estimated temperature based on an annual constant rate (Yrate.tem). The temperature series in September and October are absent at the BT AWS, and the validation of this two months are not presented in this figure.

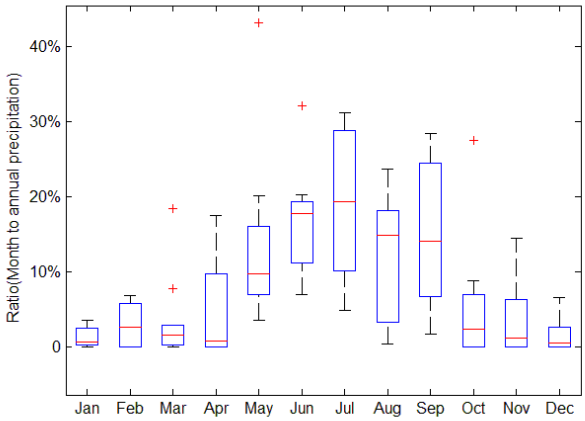

Fig. 3. Proportion of monthly precipitation to annual value (calculated for 2003 to 2012). The red line in each box represents the medians value for each month from 2003 to 2012. Red crosses indicate abnormal values that exceed 1.0 times the interquartile range. Precipitation mostly occurs in May to September and can be disregarded in other months.

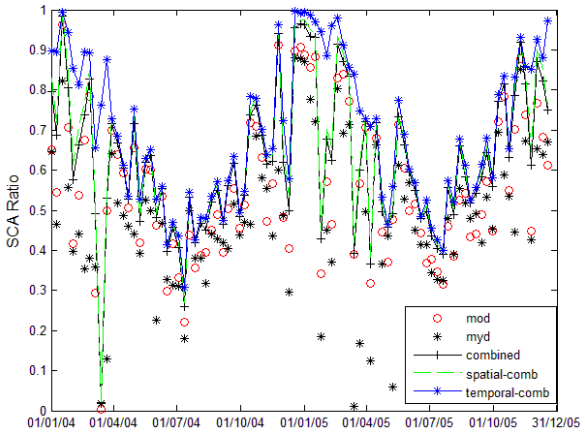

Fig. 4. Filtered MODIS eight-day snow-cover products in 2004–2005. mod is the snow cover area from MOD10A2 products, while myd is MYD10A2 products. combined is the combined result from step 1, spatial-comb from step 2 and temporal-comb from step 3. See Sect. 2.2.3 for details.

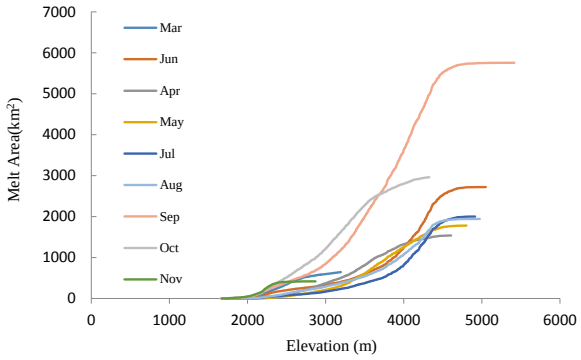

Fig. 5a. Cumulative monthly snowmelt area distribution by elevation for 2003 to 2012. The snowmelt area in December, January and February is zero and is not shown in this figure.

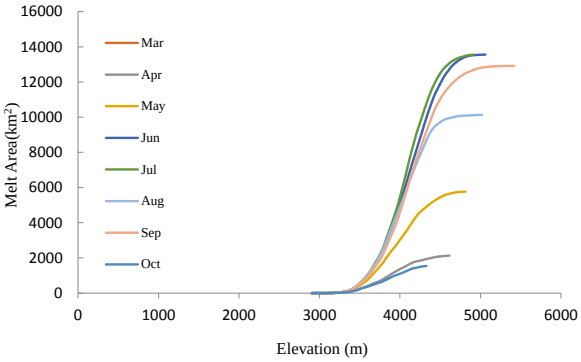

Fig. 5b. Cumulative monthly glacier melt area distribution by elevation for 2003 to 2012. The glacier melt area in November, December, January and February is zero and is not shown in this figure.

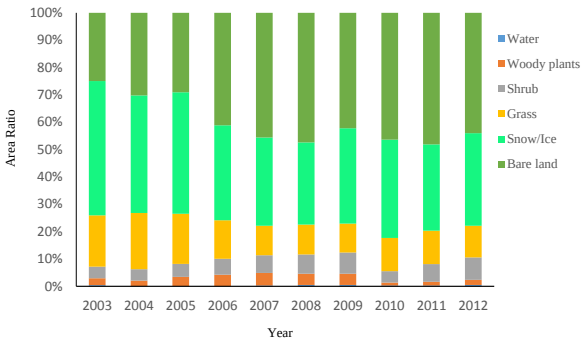

Fig. 6. Area ratio of different land cover types for 2003–2012 in the TRB.

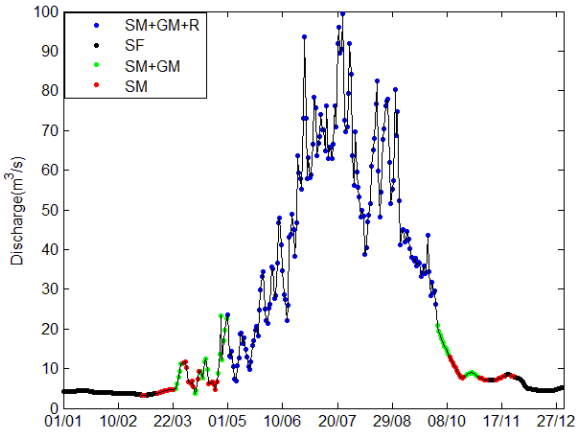

Fig. 7. Hydrograph partition of 2003.

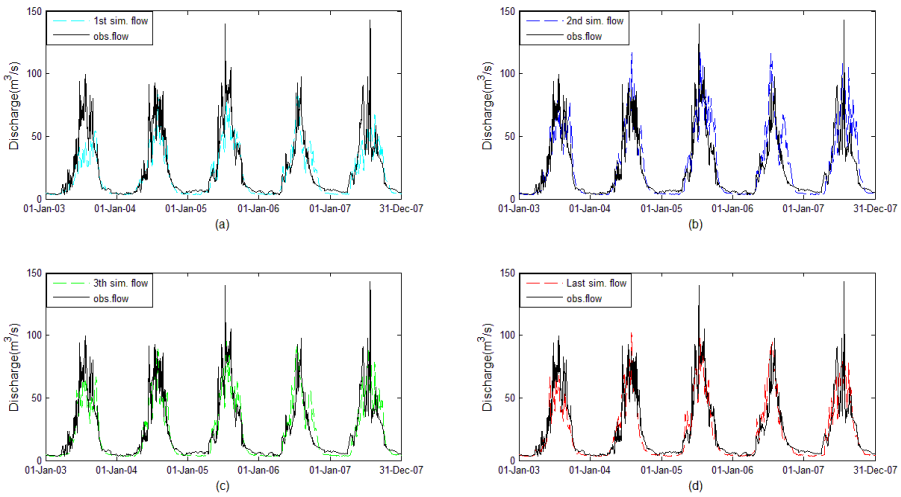

Fig. 8. Iterations of parameter calibration during 2003–2007. The first three iterations **(a–c)** and the last iteration **(d)** are presented.

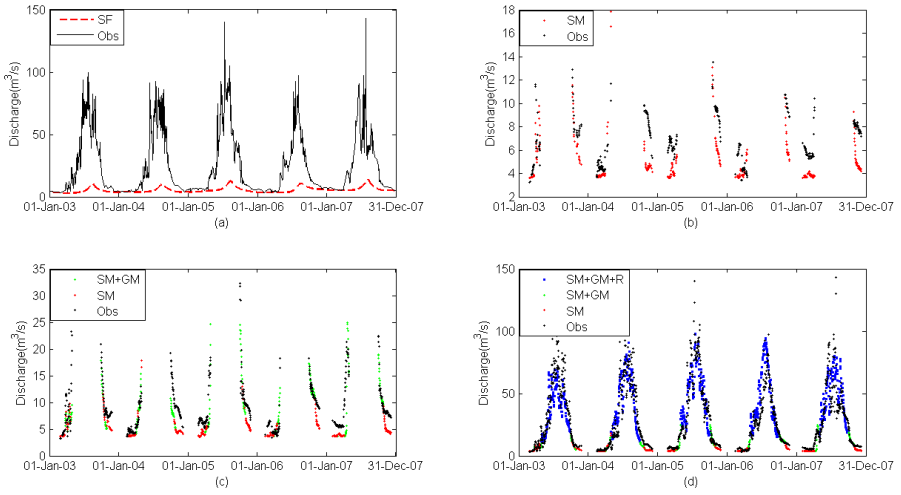

Fig. 9. (a) Estimation of groundwater baseflow (SF). **(b)** Calibration of SDDF on SM days. **(c)** Calibration of GDDF on GM + SM days. **(d)** Calibration of WM and *B* on GM + SM + *R* days.

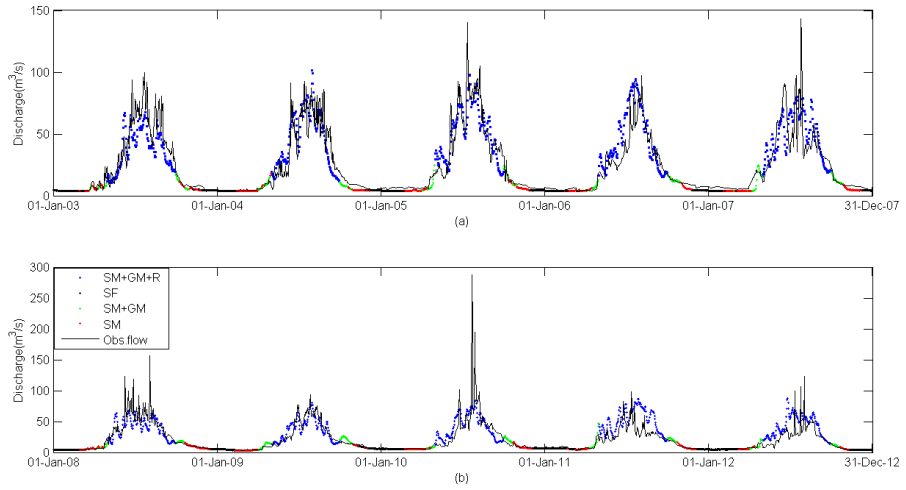

Fig. 10. (a) Simulation of each hydrograph partition in the calibration period 2003–2007. **(b)** Simulation of each hydrograph partition in the validation period 2008–2012. Partitions for the observed hydrograph are not shown.

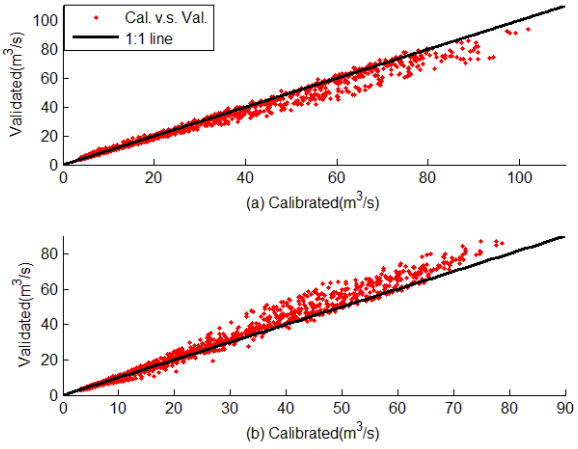

Fig. 11. Cross validation. **(a)** Simulation of 2003–2007 by parameters calibrated in 2003–2007 and 2008–2012. **(b)** Simulation of 2008–2012 by parameters calibrated in 2008–2012 and 2003–2007.